Inorganica Chimica Acta 517 (2021) 120175

Contents lists available at ScienceDirect

Inorganica Chimica Acta

journal homepage: www.elsevier.com/locate/ica

Research paper

Synthesis and antimicrobial study of organoiridium amido-sulfadoxine complexes

Timothy J. Kotzé [a], Sandra Duffy [b], Vicky M Avery [b], Audrey Jordaan [c], Digby F. Warner [c,d], Leigh Loots [a], Gregory S. Smith [e], Prinessa Chellan [a,*]

[a] Department of Chemistry and Polymer Science, Stellenbosch University, Matieland, Western Cape, South Africa
[b] Discovery Biology, Griffith Institute for Drug Discovery, Griffith University, Nathan, Queensland 4111, Australia
[c] SAMRC/NHLS/UCT Molecular Mycobacteriology Research Unit, Department of Pathology and Institute of Infectious Disease and Molecular Medicine (IDM), Faculty of Health Sciences, University of Cape Town, Cape Town, South Africa
[d] Wellcome Centre for Infectious Diseases Research in Africa (CIDRI-Africa), Faculty of Health Sciences, University of Cape Town, Cape Town, South Africa
[e] Department of Chemistry, University of Cape Town, Cape Town, South Africa

ARTICLE INFO

Keywords:
Bioorganometallic
Organoiridium
Sulfadoxine
Antimalarial
Antitubercular

ABSTRACT

Two new ligands, pyridylamido-sulfadoxine (**L1**) and quinolylamido-sulfadoxine (**L2**), were prepared by the reaction of the antimicrobial sulfadrug, sulfadoxine, with either 2-picolinic acid or 2-quinaldic acid. Subsequent reaction with a $[Cp^xIrCl_2]_2$ dimer (where Cp^x = pentamethylcyclopentadiene, tetramethylphenylcyclopentadiene or tetramethylbiphenylcyclopentadiene) yielded six new amidosulfadoxine-derivatized iridium complexes (**C1-C6**) in moderate to good yields, where the ligands act as *N,N'*-bidentate chelators. Proton and carbon NMR spectroscopy, mass spectrometry and HPLC data were used to characterize and confirm the purity of all compounds. Aquation chemistry studies on the complexes revealed slow water substitution of the chlorido ancillary ligand. The inhibitory activities of complexes **C1-C6** were determined against *Mycobacterium tuberculosis* (*Mtb*) H37Rv and *Plasmodium falciparum (Pf)* strains, 3D7, Dd2 and HB3, as well as the HEK cell line. The ligands showed no appreciable antimicrobial activity, with most of the complexes exhibiting weak to moderate inhibition of *Pf* and *Mtb*. However, one complex (**C6)** displayed potent activity against *Pf* 3D7 (IC_{50} of 0.975 μM) and the multidrug-resistant *Pf* Dd2 (IC_{50} of 0.766 μM).

1. Introduction

Tuberculosis is caused by *Mycobacterium tuberculosis (Mtb)* and is spread primarily via aerosols released by infected individuals. Approximately 1.7 billion people are infected with latent *Mtb* with 5–10% likely to develop the disease in their lifetime [1]. In 2018, an estimated 10 million new cases were reported worldwide of which South Africa contributed a major portion [1]. The decline in TB incidence rates per year is currently close to 2% which is still far too low. If definitive progress towards the eradication of this epidemic is to be made then this percentage needs to be increased nearly three-fold [1]. To further illustrate the importance of research in this field it is to be noted that, prior to the COVID-19 pandemic, *Mtb* was the leading cause of death globally owing to an infectious disease [1]. Drug-resistant TB accounts for almost a third of all antimicrobial resistant (AMR) deaths annually [2]. Multi-drug resistant TB (MDR-TB) is defined by the WHO as resistance to the two frontline drugs prescribed for standard treatment, isoniazid and rifampicin, while extensively drug resistant TB (XDR-TB) is additionally resistant to fluoroquinolones and at least one of the injectable second-line aminoglycosides [1]. The emergence and spread of drug-resistant *Mtb* strains therefore places a premium on the identification of new antimycobacterial agents that possess novel mechanisms of action and, preferably, the capacity to shorten treatment durations, currently set at a minimum six months for drug-susceptible disease.

Plasmodium parasites are the causative agents of malaria, a life-threatening infectious disease transmitted by female *Anopheles* mosquitoes that is both curable and preventable [3]. *P. falciparum* and *P. vivax* are the two species that are the most dangerous, with *P. falciparum* causing 99.7% of all malaria cases in the WHO African Region and most cases in the Eastern Mediterranean, Western Pacific and South-East Asian regions [3,4]. Although great progress was made in reducing the number of cases worldwide up till 2015, since then no

* Corresponding author.
E-mail address: p.chellan@sun.ac.za (P. Chellan).

https://doi.org/10.1016/j.ica.2020.120175
Received 20 October 2020; Received in revised form 30 November 2020; Accepted 30 November 2020
Available online 2 December 2020

significant progress has been made [4]. Children under the age of 5 are the most vulnerable group and account for 61% of the 435 000 deaths in 2017 of which 11 countries account for nearly 70%, all but 1 being in Africa. There are several approaches to targeting the parasite and preventing its transmission including malaria vector control, which consists of preventing infection by use of insecticidal mosquito nets and indoor residual spraying of insecticides [3,4].

Cases of resistance against most of the current antimalarials, including the WHO recommended artemisinin-based combination therapy, illustrate the dire need for development of new effective treatments [5,6].

The use of metals in medicine has gained significant attention owing to the incredible versatility that can be achieved by differences in oxidation state, coordination number, geometries, electronic properties and stability. Each of these can be adjusted and modified by selecting the appropriate ligands and using various synthetic methods, allowing for an incredible variety of possibilities in design [7-21]. More recently, there has been a surge of research into metal complexes of drugs that have already been used in treatments and their direct repurposing or derivatisation for other therapies [22-30]. In cases where resistance has appeared to the original therapy, the metal complex may be active and function via a different mode of action against the disease [7,9,31-33].

Sulfonamide-containing drugs have been in use as antimicrobials since the early 20th century and were some of the first chemotherapeutics to be systematically employed [7,34]. They are still prevalent in the pharmaceutical industry and are used for a wide range of treatments [35]. Sulfonamides are believed to target the synthesis of tetrahydrofolic acid, an important cofactor in the synthesis of DNA and methionine, through competitive inhibition of dihydropteroate synthase, a bacterial enzyme that produces the precursors for tetrahydrofolic acid from *para*-aminobenzoic acid [36]. Their low toxicity and affordability make them very attractive candidates for drug research and they have been found to be effective for a wide variety of treatments, having been employed as antibacterial, antiviral, antitumour and antifungal agents, to name a few [34,36-41]. Sulfadoxine (Fig. 1) in combination with pyrimethamine is still used to treat certain cases of malaria and as a preventative treatment in pregnant women [4]. They were initially employed as antitubercular drugs, but with the discovery of isoniazid, rifampicin and streptomycin, were largely made obsolete owing to their lower efficacy [42]. With the rise of drug resistance and the trend of repurposing, it could prove beneficial to relook at these pharmacophores for solutions.

Several accounts have been published reporting an increase in biological activity when a clinical drug or organic pharmacophore is incorporated into a metal complex [7,31,43-46]. This increase in activity has also been documented for sulfonamides and a range of different sulfonamide metal complexes have been developed [43,47,48]. They have been screened for a multitude of biological applications, including as anticancer [49,50], antimicrobial or antifungal agents [51,52] and, as carbonic anhydrase inhibitors (which have application to a variety of illnesses) [53-56]. Mondelli *et al.* investigated cobalt sulfonamide complexes of sulfapyridine, sulfadimethoxine, sulfamethazine, sulfamerazine, sulfamethoxazole and sulfamethizole as inhibitors of *Mtb* [57]. The complexes generally showed comparable activity to that of their metal free ligands. Studies on ferrocenyl and cyrhetrenyl sulfonamide complexes revealed moderate activity on *Mtb* strains [58].

In a previous study, we showed that the incorporation of organometallic rhodium and iridium half-sandwich moieties into the drug sulfadoxine effectively 'switched on' it's antimalarial and antitubercular activity [15]. The sulfadoxine drug on its own was not active while the complexes showed low micromolar activities. We also found that the complexes, which underwent slow exchange of the chlorido ligand with water, were better inhibitors of malarial parasite growth [15]. The iridium derivatives (Fig. 1, **C7** – **C12**) were the most promising complexes, therefore we have decided to extend our studies on organoiridium sulfadoxine complexes. The previously reported complexes **C7 – C12** were cationic complexes where the imino ligands chelated to the metal in an *N,N'*-bidentate fashion. To extend our work on organometallic sulfa-drug complexes, we wished to determine if neutral *N,N'*-chelated complexes would be more potent than the cationic analogues.

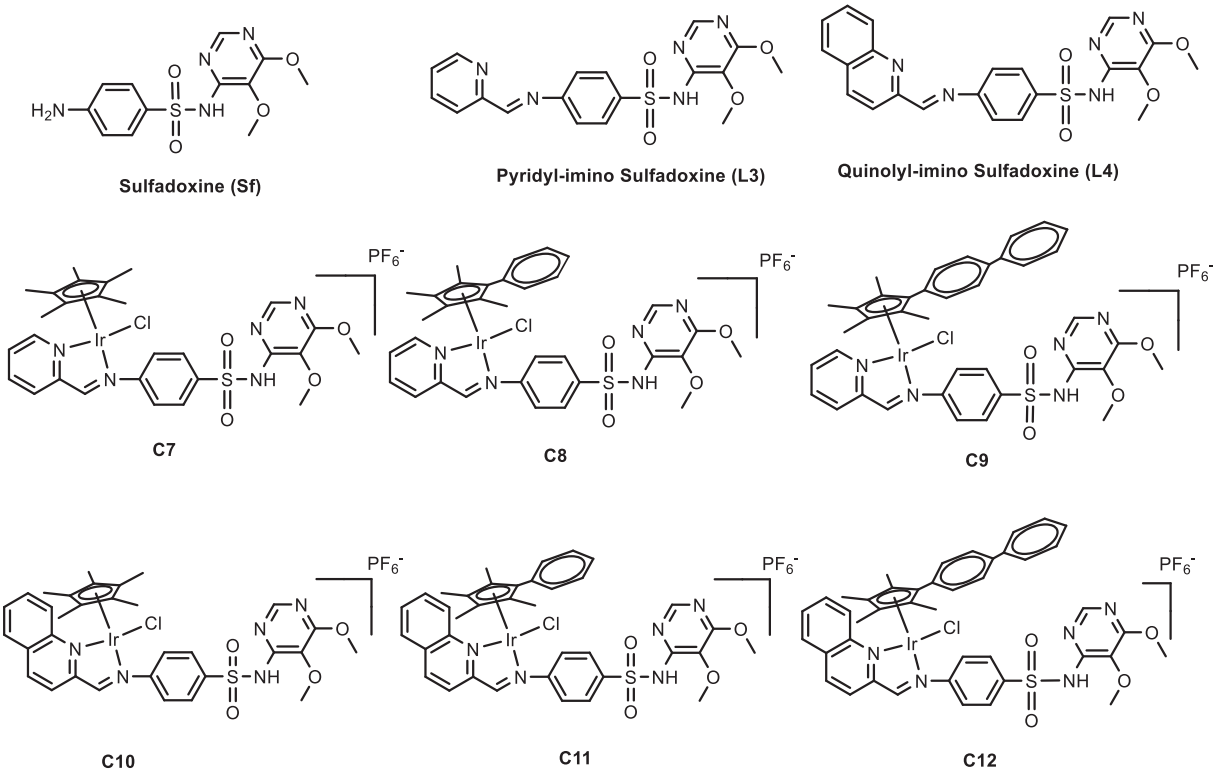

Fig. 1. Structures of Sulfadoxine (**Sf**), the imino ligands (**L3** and **L4**) and iridium(III) imino-sulfadoxine complexes (**C7 – C12**) previously studied [15].

Thus, we report the synthesis and study of a small library of new sulfadoxine iridium complexes (**C1-C6**) where the heteroaromatic-imino group of (**C7-C12**, Fig. 1) is replaced with an heteroaromatic amido group. The complexes were tested against *Plasmodium falciparum* (*Pf*) strains Dd2, 3D7 and HB3, the *Mtb* H37Rv strain and the HEK cell line in dose–response assays.

2. Results and discussion

2.1. Synthesis

The new amido ligands, **L1** and **L2**, were prepared by reaction of the corresponding acid chloride (generated *in situ*) and sulfadoxine (Scheme 1) and were obtained in moderate yields. Both ligands displayed similar absorption bands in their infrared spectra. For **L1**, the amide N—H stretch is observed at 3339 cm^{-1} with the sulfonamide N—H stretch appearing at 3165 cm^{-1}, a slightly lower frequency compared to sulfadoxine. A strong, sharp absorption band is observed for the carbonyl of the amide functional group at 1681 cm^{-1}. Further analyses with proton NMR spectroscopy show the amide proton for **L1** and **L2** resonates as singlets at 10.27 (**L1**) and 10.49 (**L2**) ppm. The proton of the carbon *ortho* to nitrogen in the pyridyl ring (**L1**) was observed as a doublet at 8.62 ppm. Some of the aromatic protons of the quinolyl ring in **L2** overlap, making it difficult to discern if the *ortho* proton also resonates as a doublet as expected. ^{13}C NMR spectroscopy revealed that the amide carbon resonates at *ca.* 162 ppm for both ligands. These shifts agree with similar pyridyl amide compounds reported [59,60]. The ligands were also subjected to mass spectral analysis using ESI-MS and the base peak observed corresponds to the $[M]^+$ molecular ion.

Crystals of **L1** were obtained by layering a dichloromethane solution of the ligand with hexane and leaving to stand in a sealed vial for several days at room temperature. The molecular structure for **L1** is shown in Fig. 2. The needle-like crystals were transparent and crystallised in the triclinic space group, $P\bar{1}$. General crystal data and selected bond lengths and angles are given in Tables 1 and 2. The bond lengths and angles determined for **L1** were similar for other sulfonamide-containing structures in the literature [61,62].

Complexes **C1-C6** were prepared using a microwave synthetic method. Ligands, **L1** or **L2**, were combined with the appropriate iridium dimer and sodium bicarbonate in methanol (Scheme 2) and subjected to microwave irradiation for 10 min at 150 °C, resulting in isolation of the complexes as either yellow or orange amorphous solids in moderate to high yields.

Characterisation data for all complexes were similar, therefore complex **C1** is discussed as a representative example. The IR spectrum of **C1** revealed a large shift in the carbonyl signal to 1621 cm^{-1} from 1681 cm^{-1} in the ligand (**L1**). Additionally, no absorption band was observed for the NH stretch of the amide (observed at 3339 cm^{-1} for L1). The C═N stretch of the pyridyl ring shifts from 1584 cm^{-1} to 1603 cm^{-1}, indicative of coordination through the nitrogen atoms of the pyridyl ring and the amide.[28,29] The shift to low frequency of the ν(CO) stretch and to high frequency of the pyridyl ν(C═N) stretch is a consequence of the back-bonding between the nitrogen and Ir metal center. This results in greater donation of electron-density from the C═O group into the pyridyl ring, thus weakening the C═O bond and strengthening the C═N bond despite the M–N bond formed. The band at 1525 cm^{-1} seen in the spectrum for **L1** and attributed to the amide N—H bend, is not observed for **C1** further confirming deprotonation of the amide nitrogen prior to complexation. As the electronegativity of the metal centre increases within the series, there is a slight general shift to higher frequencies for all the bands observed. In particular, for complexes **C4-C6**, the quinolyl C═N stretch combines with the C═O stretch to form a broad band which could not be separately identified.

Formation of **C1** is further confirmed by the absence of the amide NH peak from the ^1H NMR spectrum. Upon complexation, the changes in chemical shifts compared to **L1** are not large, with the proton of the carbon *ortho* to the nitrogen of the pyridyl ring shifting from 8.62 ppm to 8.58 ppm. The protons for the methyl groups of the Cp* ring resonate at 1.38 ppm. The complexes containing the Cp^{xph} or Cp^{xbiph} ligand (**C2**, **C3**, **C5** and **C6**) display separate methyl peaks for the coordinating Cp^x moiety. This is the result of the inequivalence introduced by the attached phenyl or biphenyl ring along with the induced chirality of the metal

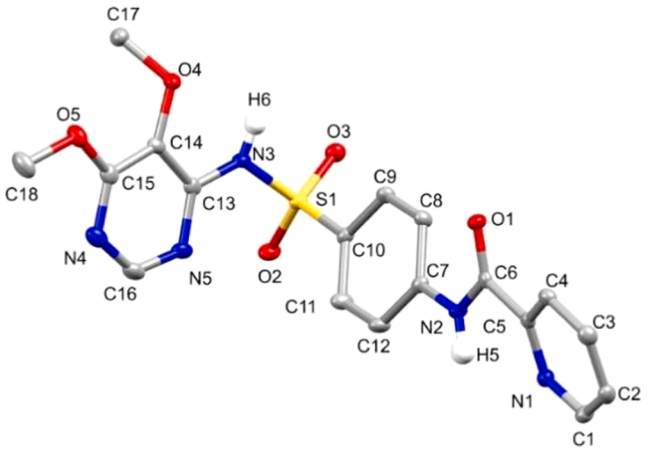

Fig. 2. Molecular structure of **Amido-Sf-L1** with atom labelling. ORTEP thermal ellipsoids are drawn at 50% probability level. Hydrogen atoms (with the exception of H5 and H6) have been omitted for clarity.

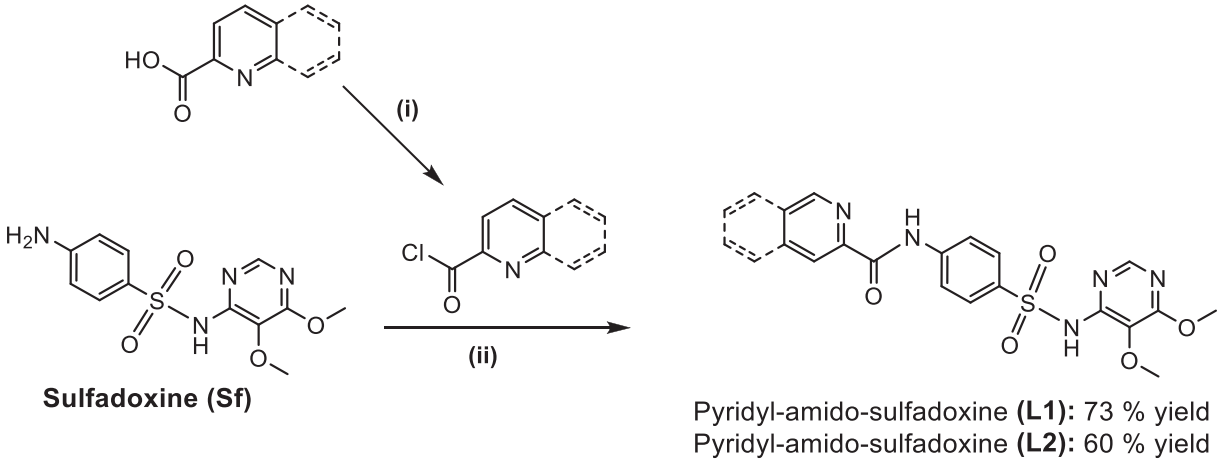

Scheme 1. Synthesis of **L1** and **L2** via an acid chloride. (i) oxalyl chloride / cat. DMF / 2–5 h, 0 °C / dichloromethane; (ii) 2–3 h, Pyridine, rt, Acetonitrile.

Table 1
Crystal data and structure refinement for **L1**.

Empirical formula	$C_{18}H_{17}N_5O_5S$
Formula weight	415.42
Temperature (K)	100(2)
Wavelength (Å)	0.71073
Crystal system	Triclinic
Space group	$P\bar{1}$
Unit cell dimensions (Å, °)	a = 8.319(2), α = 109.559(4); b = 10.194(3), β = 100.736(4); c = 12.280(3), γ = 103.451(4)
Volume (Å)	913.9(4)
Z	*2*
Calculated density (g cm^{-3})	1.51
Absorption coefficient (mm^{-1})	0.221
F000	432
Crystal size (mm^3)	0.118 × 0.073 × 0.048
θ range for data collection (θ)	1.838 to 27.572
Miller index ranges	$-10 \leq h \leq 10$ $-15 \leq l \leq 15$ $-13 \leq k \leq 13$
Reflections collected	24,537
Independent reflections	4207 [R_{int} = 0.0496]
Completeness to θmax (%)	0.998
Max. and min. transmission	0.9354 and 1.000
Refinement method	Full-matrix least-squares on F^2
Data / restraints / parameters	4207 / 0 / 272
Goodness-of-fit on F^2	1.045
Final R indices [I > 2σ(I)]	R1 = 0.0402 wR2 = 0.0970
R indices (all data)	R1 = 0.0512 wR2 = 0.1028
Largest diff. peak and hole (e $Å^{-3}$)	0.508 and −0.443

Table 2
Selected bond lengths and angles for **L1.**

Bond Length	**Length (Å)**
N2– C6	1.358(2)
O1-C6	1.230(2)
C7-N2	1.407(3)
C6-C5	1.501(3)
C10-S1	1.761(2)
S1-O3	1.434(1)
S1-O2	1.429(1)
S1-N3	1.649(2)
N3-C13	1.396(2)
O5-C15	1.339(3)
C14-O4	1.372(2)
H6-N3	0.84(2)
H5-N2	0.84(3)
Bond angles	**Angle (°)**
O3-S1-O2	119.55(9)
O3-S1-N3	103.45(9)
O3-S1-C10	108.58(9)
O2-S1-N3	109.32(9)
O2-S1-C10	109.29(9)
N3-S1-C10	105.71(9)
C7-N2-C6	126.9(2)
C7-N2-H5	117(2)
C6-N2-H5	116(2)
S1-N3-C13	125.5(1)
S1-N3-H6	110(2)
C13-N3-H6	118(2)
Torsion Angles	**(°)**
C4-C5-C6-N2	−166.8(2)
C6-N2-C7-C8	21.6(3)
S1-N3-C13-N5	−13.1(3)
N3-S1-C10-C11	105.9(2)

centre. As the length of the Cp^x moiety is extended with a phenyl (Cp^{xph}) and biphenyl (Cp^{xbiph}), the protons of these added phenyl rings resonate between 7.30 ppm and 7.70 ppm. In the ^{13}C spectrum, the quaternary carbons of the Cp^x ring appear as one singlet for **C1** and **C4** and as separate peaks for complexes ***C2***, **C3**, **C5** and **C6**. The ESI-MS spectra for all complexes displayed a base peak that corresponds to the $[M-Cl]^+$ molecular ion. The purity of all ligands and complexes was determined by HPLC to be between 95 and > 99%. Together, the mass spectral and HPLC data obtained confirms only one species was present for each compound with no impurities.

2.2. Aquation chemistry for C1-C6

Given the aqueous environment that drugs are administered or screened in, it is important to study the speciation of potential metallodrugs in water. All of the complexes contain a chlorido ligand that could be displaced by water in aqueous media. In order to study the aquation of complexes **C1-C6**, we used two approaches. First, *in situ* reaction of the appropriate complex with an excess of deuterium oxide at 37 °C in the presence of an equimolar amount of $AgNO_3$ to make sure that the deuterium oxide complexes (**C1-*D*$_2$*O*** – **C6-*D*$_2$*O***) were prepared. Second, complexes **C1-C6** were incubated in deuterium oxide without $AgNO_3$ at 37 °C to determine whether complexes would undergo aquation without the presence of a halide abstraction reagent. After filtration and addition of TMS as internal standard, solutions were analysed using proton NMR spectroscopy. It was assumed that any material soluble in D_2O was a deuterium oxide species (all chlorido complexes are insoluble in water), where a deuterium molecule coordinates to the metal centre, forming a cationic complex with NO_3^- as the counterion. The overlaid spectra of **C1-*D*$_2$*O*** and **C1** after incubation without $AgNO_3$ are shown in Fig. 3. Spectra for the other complexes are shown in the supplementary data (Figs. S1-S5).

It is clear from the NMR spectra that complex **C1** does not undergo aquation after 18 h in the absence of $AgNO_3$. The proton *ortho* to the nitrogen of the pyridyl ring for **C1-*D*$_2$*O*** (Fig. 3, Blue spectrum) is seen at 9.01 ppm, while that of the incubated **C1** resonates at 8.91 ppm. Similar observations were made for complexes ***C2*** and **C4**. Complex **C3** did not undergo aquation in presence of $AgNO_3$ even at increased temperatures of 45 – 50 °C, and it is likely that the steric bulk of the biphenyl moiety bound to the metal centre prevents access to the chlorido ligand. The lack of aquation of **C3** was confirmed with MS. For complex **C5**, the species in solution was too dilute and no definitive assignments could be made from the spectra. **C6** was extremely insoluble under the conditions used and based on the results for aquation of **C3**, it was assumed that similar results would be obtained.

The results of the aquation studies show that the chlorido was either not displaced by D_2O or was extremely slow in being substituted. This suggests that, during the *in vitro* inhibitory experiments, the active species of complexes **C1-C6** is most likely either the chlorido derivatives or that the complexes remain intact long enough to reach their target before undergoing aquation.

2.3. In vitro antimycobacterial screening

Complexes **C1-C6** were screened for activity against the *Mtb* H37Rv strain. For the anti-tubercular studies, the minimum inhibitory concentration that inhibits 90% of cell growth (MIC_{90}) of *Mtb* H37Rv was determined using two different media (Table 3), one enriched with casitone, glucose and tyloxapol (7H9 CAS GLU Tx) and the other with ADC (albumin-dextrose-catalase), glucose and Tween80 (7H9 ADC GLU Tw).

No activity is observed when the compounds are tested in the media enriched with ADC, demonstrating that the activities of these compounds are sensitive to the type of media used. The data from experiments using the 7H9 CAS GLU Tx medium shows only **C1**, **C3** and **C4** having any detectable activity after 14 days. **C3** was the best inhibitor with a MIC_{99} of 34.3 μM after 14 days. As antimycobacterial agents, these compounds are not very effective *in vitro*.

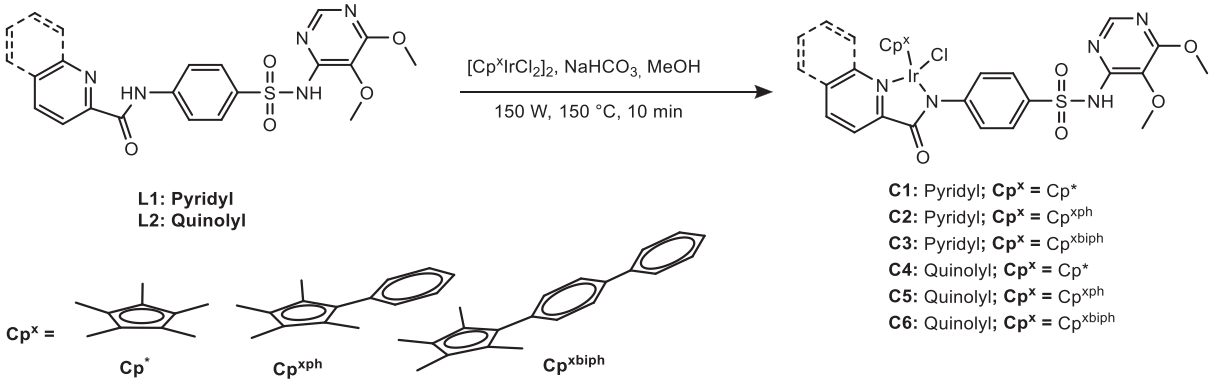

Scheme 2. General synthetic procedure for the complexes **C1-C6**.

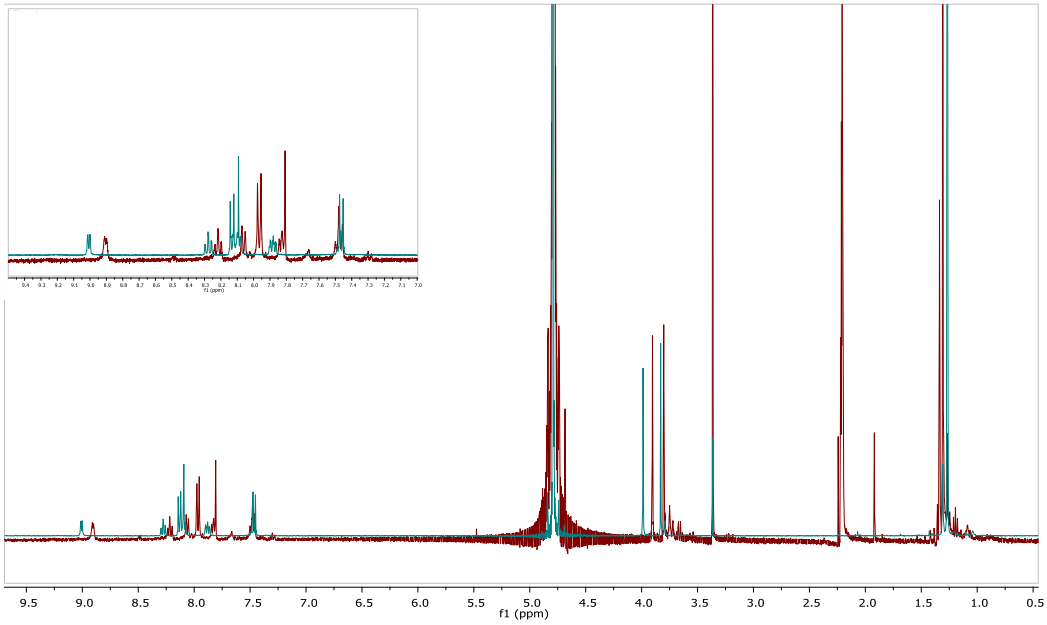

Fig. 3. Aqua species of **C1-*D_2O*** (Blue), prepared by incubation with silver nitrate, overlaid with the incubated chlorido species of **C1** (Red) with no silver nitrate. Both spectra are referenced to TMS. (For interpretation of the references to colour in this figure legend, the reader is referred to the web version of this article.)

Table 3
MIC_{90} data for **L1, L2, C1-C6,** and the control drug, rifampicin (**Rfm**) against *Mtb* H37Rv.

Compound	7H9 CAS GLU Tx[a]	7H9 ADC GLU Tw[b]		
	Day 7 (μM)[c]	**Day 14 (μM)**[c]	**Day 7 (μM)**[c]	**Day 14 (μM)**[c]
L1	n.a[d]	n.a[d]	n.a[d]	n.a[d]
L2	n.a[d]	n.a[d]	n.a[d]	n.a[d]
C1	n.a[d]	80.4	n.a[d]	n.a[d]
C2	n.a[d]	n.a[d]	n.a[d]	n.a[d]
C3	68.3	34.3	n.a[d]	n.a[d]
C4	n.a[d]	75.5	n.a[d]	n.a[d]
C5	n.a[d]	n.a[d]	n.a[d]	n.a[d]
C6	n.a[d]	n.a[d]	n.a[d]	n.a[d]
Rfm	0.032	0.016	0.004	0.005

[a] Middlebrook 7H9 media supplemented with casitone, glucose and tyloxapol
[b] Middlebrook 7H9 media supplemented with ADC (albumin-dextrose-catalase), glucose and Tween80.
[c] MIC_{90} values were determined in μg/ml and converted to μM.
[d] Not active up to the highest concentration tested (125 μg/ml).

2.4. In vitro antiplasmodial evaluation and cytotoxicity

Complexes **C1-C6** and their corresponding metal-free ligands were evaluated for their *in vitro* antiplasmodial activity against *Plasmodium falciparum* malarial parasite strains 3D7 (CQ-sensitive and sulfadoxine-resistant), Dd2 (multidrug resistant strain) and HB3 (pyrimethamine-resistant and CQ-sensitive strain). The percentage inhibition at a compound concentration of 80 μM was first determined to ascertain if the complexes show activity (Fig. 4 and Table S1 in supplementary information). Both ligands, **L1** and **L2**, show no appreciable inhibition. For the complexes, a general increase in percentage inhibition was observed when moving from the pyridyl (**C1-C3**) to the quinolyl systems (**C4-C6**). When comparing the percentage inhibitions, **C4** (92.4% (3D7), 92.7% (Dd2), 87.1% (H3B)) and **C6** (97.1% (3D7), 96.7% (Dd2), 91.8% (H3B)) show consistently high inhibition across all *Pf* strains (Table 4). These complexes were also less cytotoxic on the non-tumorigenic HEK cell line. Based on our previous study of the imino derivatives [15], where we observed a distinct increase in activity based on 'hydrophobicity', we hypothesised a similar trend for complexes **C1-C6**. However, from the percentage inhibition data, we see no discernible trend in the activities based on structure. The pyridyl Cp^{xph} complex, **C2**, was essentially inactive across all three parasite strains while the quinolyl Cp^{xph} complex, **C5**,

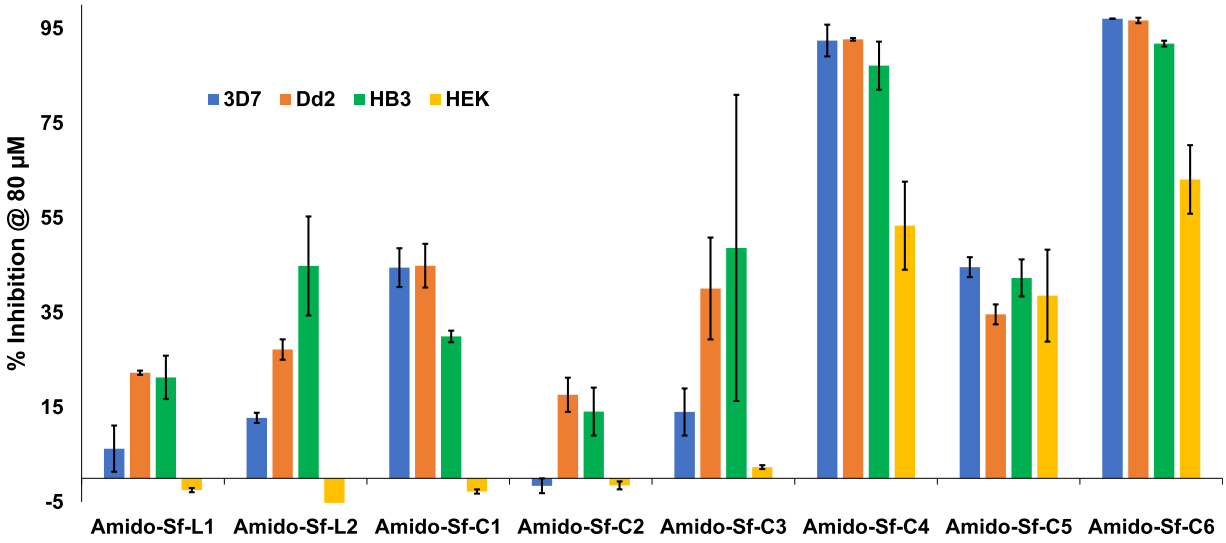

Fig. 4. Percent inhibition data for the ligands (**L1** and **L2**) and complexes (**C1-C6**) on the *Pf* parasite **3D7** (CQ-sensitive and sulfadoxine-resistant), **Dd2** (multidrug resistant strain) and **HB3** (pyrimethamine-resistant and CQ-sensitive) strains and HEK (human embryonic kidney) cell line.

Table 4
IC_{50} data for **C6, C12** [15]**,** sulfadoxine **(sf)** [15] and control drugs Chloroquine (**CQ**), Puromycin (**PMN**), Artemisinin (**ART**), Pyrimethamine (**PYM**) against *Pf* parasite **3D7** (CQ-sensitive and sulfadoxine-resistant), **Dd2** (multidrug resistant strain) and **HB3** (pyrimethamine-resistant and CQ-sensitive) strains.

Compound	3D7[a] IC_{50}	Dd2[a] IC_{50}	H3B[a] IC_{50}
C6	0.78 (0.142)	1.09 (0.23)	0.83 (0.08)
C12[b]	0.25 (0.04)	0.17 (0.07)	n.t[c]
Sf[b]	> 20 µM	> 20 µM	n.t[c]
CQ	0.036 (0.014) nM	0.205 (0.004) nM	0.048 (0.005) nM
PMN	0.057 (0.003) nM	0.063 (0.002) nM	0.099 (0.004) nM
ART	0.005 (7.743×10^{-4}) nM	0.005 (1.414×10^{-4}) nM	0.003 (6.364×10^{-4}) nM
PYM	0.003 (1.48×10^{-4}) nM	43% at 4µM[d]	86.5% at 4 µM[d]

[a] Standard error is given in parentheses.
[b] Data from reference [15].
[c] Not tested.
[d] percent inhibition tested at 4 µM.

was moderately active (44.6% (3D7), 34.6% (Dd2), 42.3% (H3B)).

The two complexes showing the best percentage inhibition (**C4** and **C6**) were assayed to determine their IC_{50}-values on the *Pf* strains. However, at the time of testing, the IC_{50} for **C4** could not be determined as its sigmoidal dose response curve did not give a plateau and it was therefore considered inactive. The sub–micromolar IC_{50}-values observed for complex **C6** (IC_{50} = 0.78 (3D7), 1.09 (Dd2), 0.83 (H3B) µM) show it to be the most promising complex in the amido-sulfadoxine complex library. However, it is not as active as its imino derivative (**C12**) [15]. It's clear that the amido-sulfadoxine complexes (**C1-C6**) reported here are not as potent as their imino-sulfadoxine counterparts (**C7-C12**) previously studied [15].

3. Conclusions

Two new ligands – pyridylamido-sulfadoxine (**L1**) and quinolylamido-sulfadoxine (**L2**) – were successfully synthesized along with their organoiridium complexes (**C1-C6**). Spectral characterisation and the crystal structure for **L1** confirmed the structural integrity of these compounds. The aquation studies showed an increased difficulty in removal of the chlorido ligand as the bulk of the half-sandwich moiety increased, especially for the tetramethylbiphenylcyclopentadiene analogues (**C3** and **C6**), suggesting that the active species is the chlorido complex. With the exception of **C6**, all of the complexes displayed very low activities on the *Mycobacterium tuberculosis* and *plasmodium falciparum* strains studied. No trend in activity could be linked to the aqueous solubility or structures of the amido complexes against malaria. **C6** was revealed to be the most promising antimalarial with IC_{50}'s $\leq$ 1.0 µM against the three *Pf* strains assayed.

4. Experimental Section.

4.1. Chemicals and reagents

Sulfadoxine (95%), 2-picolinic acid, quinaldic acid, salicylaldehyde, 2-hydroxynapthaldehyde, oxalyl chloride (2 M in dichloromethane), pyridine, magnesium sulfate, sodium bicarbonate, 1,2,3,4,5-pentamethylcyclopentadiene, 2,3,4,5-tetramethyl-2-cyclopentenone, phenyl magnesium bromide (1 M in THF), silver nitrate, hydrocortisone, reserpine, phosphate buffered saline tablets and all reagent solvents and deuterated solvents (dimethylsulfoxide-d_6 and chloroform-d_1) were obtained from Sigma Aldrich (Merck). $IrCl_3{\cdot}nH_2O$ was purchased from Heraeus South Africa. All purchased reagents were used as received. Dichloro(pentamethylcyclopentadienyl)iridium(III) dimer, dichloro (tetramethylphenylcyclopentadienyl)iridium(III) dimer and dichloro (tetramethylbiphenylcyclopentadienyl)iridium(III) dimer were synthesized according to a literature method [63].

4.2. Instrumentation

IR spectroscopy was performed using a Thermo Nicolet Nexus 470 by means of potassium bromide pellets. NMR data (^1H, ^{13}C) were recorded on either a 300 MHz Varian VNMRS or a 400 MHz Varian Unity Inova spectrometer. ^1H NMR chemical shifts are reported in ppm and coupling constants in Hertz and were internally referenced to dimethylsulfoxide-d_6 (2.50 ppm) or chloroform-d_1 (7.26 ppm). Data was processed using MestReNova 11.0.4–18998. Mass spectrometry was performed on a Waters Synapt G2 with an ESI probe in ESI Positive mode using a Cone Voltage of 15 V. Microwave syntheses were carried out in a CEM Discover SP microwave reactor. UV–vis data were recorded with a Shimadzu UV–vis spectrophotometer.

4.3. Synthesis of pyridylamido-sulfadoxine (L1)

2-Picolinic acid (103 mg, 0.837 mmol) was stirred in dry dichloromethane (20.0 mL) under nitrogen and cooled to 0 °C. Oxalyl chloride

(2 M in dichloromethane, 484 μL, 0.966 mmol) was then added to the solution followed by a catalytic amount of dimethylformamide (50.0 μL). The reaction solution was stirred for 2 h at 0 °C before the solvent was removed and the crude residue re-dissolved in acetonitrile (10.0 mL) and cooled again to 0 °C. Sulfadoxine (200 mg, 0.644 mmol) was added dropwise (10.0 mL) over 5 min and pyridine (77.8 μL, 0.966 mmol) was added. The reaction solution was stirred at 0 °C for 30 min and for a further 1.5 h at room temperature. The purple precipitate formed was filtered, washed with acetonitrile and kept aside. The solvent was removed from the filtrate and the crude residue re-dissolved in dichloromethane (20.0 mL). This was washed with a solution of saturated sodium bicarbonate (3 × 10.0 mL) and the organic portions dried over $MgSO_4$. The solvent was evaporated, and the off-white powder obtained was combined with the purple precipitate and recrystallised from dichloromethane /hexane and washed with acetonitrile to give **L1** as a pure white powder in 67% yield (979 mg). ^{1}H NMR (300 MHz, $CDCl_3$): δ_H 10.27 (s, 1H, amide-NH), 8.62 (d, 1H, ^3J = 4.7 Hz, pyridyl-H), 8.29 (d, 1H, ^3J = 7.8 Hz, pyridyl-H), 8.20–8.14 (m, 3H, pyrimidine-H and phenyl-H), 7.97–7.90 (m, 3H, pyridyl-H and phenyl-H), 7.82 (s, 1H, sulfonamide-H), 7.55–7.49 (m, 1H, pyridyl-H), 3.97 (s, 3H, CH_3), 3.86 (s, 3H, CH_3). ^{13}C NMR (75 MHz, $CDCl_3$): δ_C 162.3, 160.8, 149.7, 149.0, 148.1, 142.3, 137.9, 134.0, 130.0, 127.0, 126.5, 122.6, 119.0, 60.6, 54.1. FT-IR (KBr, cm^{-1}) υ = 1681 (C═O), 1584 (C═N), 1525 (C═N), 3339 (N—H), 3165 (N—H). (+)-HR-ESI-MS: *m/z* (%) 416.1023 ($[M+H]^+$, 100%), 438.0841 ($[M+Na]^+$, 5%); HPLC purity: 97%; $t_{r'}$ = 15.08 min.

4.4. Synthesis of quinolylamido-sulfadoxine (*L2*)

Quinaldic acid (109 mg, 0.628 mmol) was stirred in dry dichloromethane (15.0 mL) under nitrogen and cooled to 0 °C. Oxalyl chloride (2 M in dichloromethane, 362 μL, 0.725 mmol) was then added followed by a catalytic amount of dimethylformamide (50.0 μL). The solution was stirred for 5 h at 0 °C before the solvent was removed and the crude residue re-dissolved in acetonitrile (10.0 mL) and cooled again to 0 °C. Sulfadoxine (150 mg, 0.483 mmol) was then added dropwise (10.0 mL) over 5 min and then pyridine (58.4 μL, 0.725 mmol). The reaction solution was stirred at 0 °C for 30 min before stirring a further 2.5 h at room temperature. The solvent was removed from the reaction mixture and the crude residue re-dissolved in dichloromethane (20.0 mL) and washed with saturated sodium bicarbonate (3 × 10.0 mL), distilled water (3 × 10.0 mL) and brine (2 × 10.0 mL). The solvent was removed, and the residue left to dry overnight on the high vacuum pump before being re-dissolved in dichloromethane and filtered through celite™ to remove any residual NaCl. Evaporation of the solvent yielded the crude product that was recrystallised from dichloromethane /hexane (1:2) to give **L2** as a pure off-white microcrystalline solid in 60% yield (134 mg). ^{1}H NMR (400 MHz, $CDCl_3$): δ_H 10.49 (s, 1H, amide-NH), 8.42–8.36 (m, 2H, quinolyl-H), 8.24–8.16 (m, 4H, quinolyl-H, pyrimidine-H and phenyl-H), 8.02 (d, 2H, ^3J = 8.8 Hz, phenyl-H), 7.94 (d, 1H, ^3J = 8.2 Hz, quinolyl-H), 7.87–7.81 (m, 1H, quinolyl-H), 7.79 (s, 1H, sulfonamide-NH), 7.82–7.65 (m, 1H, quinolyl-H), 3.98 (s, 3H, CH_3), 3.87 (s, 3H, CH_3). ^{13}C NMR (101 MHz, $CDCl_3$): δ_C 162.67, 160.97, 149.88, 148.95, 146.39, 142.48, 138.30, 134.19, 130.75, 130.18, 129.79, 129.77, 128.69, 128.03, 126.58, 119.20, 118.83, 60.72, 54.30. FT-IR (KBr, cm^{-1}) υ = 1679 (C═O), 1577 (C═N), 1531 (C═N), 3287 (N—H), 3177 (N—H). (+)-HR-ESI-MS: *m/z* (%) 466.1179 ($[M+H]^+$, 100%), 488.1001 ($[M+Na]^+$, 2%). HPLC purity: 98%; $t_{r'}$ = 20.51 min.

4.5. General method for synthesis of complexes *C1-C6*

The appropriate ligand (2 mol equiv.) was added to a stirred suspension of the appropriate iridium metal dimer (1 mol equiv.) and $NaHCO_3$ (2 mol equiv.) in dry methanol in a microwave vial. The vial was then sealed and placed in the microwave reactor and heated to 150 °C for 10 min at 150 W, after which, any effervescence was allowed to subside before the vial was opened and cooled to room temperature. The resulting solid was filtered and washed with Methanol/Ether before it was recrystallised from dichloromethane/hexane to afford the pure product.

4.5.1. *C1*

Dichloro(pentamethylcyclopentadienyl)iridium(III) dimer (50.0 mg, 0.0628 mmol), **L1** (52.1 mg, 0.126 mmol), and $NaHCO_3$ (10.5 mg, 0.126 mmol) was reacted in methanol (1.50 mL) in a 10.0 mL microwave vial to afford complex **C1** as a yellow powder in 84% yield (82.8 mg). ^{1}H NMR (400 MHz, $CDCl_3$): δ_H 8.58 (d, 1H, ^3J = 5.6 Hz, pyridyl-H), 8.19–8.07 (m, 4H, pyrimidine-H, pyridyl-H, phenyl-H), 7.94 (t, 1H, ^3J = 7.7 Hz, pyridyl-H), 7.87 (d, 2H, ^3J = 8.8 Hz, phenyl-H), 7.53 (m, 1H, pyridyl-H), 3.97 (s, 3H, CH_3), 3.84 (s, 3H, CH_3), 1.38 (s, 15H, Cp*–CH_3). ^{13}C NMR (101 MHz, DMSO): δ_C 167.86, 161.52, 153.46, 152.99, 151.40, 150.62, 139.42, 134.79, 128.59, 127.48, 127.12, 126.81, 125.43, 86.39, 60.26, 54.04, 7.93. FT-IR (KBr, cm^{-1}): ν = 1619 (C═O), 1599 (C═N), 1577 (C═N), 1561 (C═N). (+)-HR-ESI-MS: *m/z* (%) 742.1687 ($[M-Cl]^+$, 100%), 778.1456 ($[M+H]^+$, 2%). HPLC purity: 96.7%; $t_{r'}$ = 10.93 min.

4.5.2. *C2*

Dichloro(tetramethylphenylcyclopentadienyl)iridium(III) dimer (50.0 mg, 0.054 mmol), **L1** (45.1 mg, 0.109 mmol) and $NaHCO_3$ (9.10 mg, 0.109 mmol) were reacted together in methanol (1.50 mL) to afford complex **C2** as a bright yellow powder in 75% yield (68.7 mg). ^{1}H NMR (300 MHz, $CDCl_3$) δ_H 8.28 (d, 1H, ^3J = 5.4 Hz, pyridyl-H), 8.19–8.07 (m, 4H, pyridyl-H, pyrimidine-H, phenyl-H), 7.94 – 7.86 (m, 1H, pyridyl-H), 7.82 (d, 2H, ^3J = 8.6 Hz, phenyl-H), 7.49–7.38 (m, 5H, Cp^x-phenyl-H), 7.38–7.34 (m, 1H, pyridyl-H), 3.98 (s, 3H, CH_3), 3.85 (s, 3H, CH_3), 1.70 (s, 3H, Cp^x-CH_3), 1.48 (s, 3H, Cp^x-CH_3), 1.21 (s, 3H, Cp^x-CH_3), 1.12 (s, 3H, Cp^x-CH_3). ^{13}C NMR (101 MHz, $CDCl_3$) δ_C 168.69, 160.77, 154.54, 153.19, 149.88, 149.78, 138.80, 134.12, 130.16, 130.06, 129.16, 128.80, 128.62, 127.77, 127.21, 126.67, 126.42, 99.00, 92.58, 86.04, 82.64, 81.65, 60.55, 54.10, 9.71, 9.38, 8.52, 8.09. FT-IR (KBr, cm^{-1}): ν = 1623 (C═O), 1600 (C═N), 1577 (C═N), 1560 (C═N). (+)-HR-ESI-MS: *m/z* (%) 804.1844 ($[M-Cl]^+$, 100%), 840.1575 ($[M+H]^+$, 2%). HPLC purity: 97%, $t_{r'}$ = 13.79 min.

4.5.3. *C3*

Dichloro(tetramethylbiphenylcyclopentadienyl)iridium(III) dimer (50.0 mg, 0.0470 mmol), **L1** (38.7 mg, 0.0930 mmol) and $NaHCO_3$ (7.80 mg, 0.0930 mmol) were reacted together in methanol (1.50 mL) to afford complex **C3** as a light-yellow powder in 65% yield (55.9 mg). ^{1}H NMR (300 MHz, $CDCl_3$): δ_H 8.32 (d, 1H, ^3J = 5.5 Hz, pyridyl-H), 8.19–8.09 (m, 4H, pyrimidine-H, phenyl-H, pyridyl-H), 7.94 – 7.87 (m, 1H, pyridyl-H), 7.84 (d, 2H, ^3J = 8.9 Hz, phenyl-H), 7.67–7.61 (m, 4H, Cp^x-phenyl-H), 7.58–7.32 (m, 6H, Cp^x-phenyl-H), 3.98 (s, 3H, CH_3), 3.85 (s, 3H, CH_3), 1.74 (s, 3H, Cp^x-CH_3), 1.49 (s, 3H, Cp^x-CH_3), 1.27 (s, 3H, Cp^x-CH_3), 1.11 (s, 3H, Cp^x-CH_3). ^{13}C NMR (75 MHz, $CDCl_3$): δ_C 168.84, 160.91, 154.62, 153.30, 150.07, 149.94, 141.41, 140.03, 138.97, 134.34, 130.59, 129.22, 129.10, 128.90, 127.98, 127.95, 127.84, 127.34, 127.04, 126.77, 126.59, 99.22, 92.76, 86.10, 82.90, 81.39, 60.67, 54.21, 9.89, 9.57, 8.64, 8.17. FT-IR (KBr, cm^{-1}): υ 1618 (C═O), 1598 (C═N), 1580 (C═N), 1661 (C═N). (+)-HR-ESI-MS: *m/z* (%) 880.2172 ($[M - Cl]^+$, 100%), 916.1915 ($[M+H]^+$, 2%) HPLC purity: 97.9%; $t_{r'}$ = 18.07 min.

4.5.4. *C4*

Dichloro(pentamethylcyclopentadienyl)iridium(III) dimer (50.0 mg, 0.0630 mmol), **L2** (58.4 mg, 0.126 mmol) and $NaHCO_3$ (10.6 mg, 0.126 mmol) were reacted in methanol (1.50 mL) to afford complex **C4** as an orange powder in 77% yield (80.5 mg). ^{1}H NMR (400 MHz, $CDCl_3$): δ_H 8.60 (d, 1H, ^3J = 8.7 Hz, quinolyl-H), 8.34 (d, 1H, ^3J = 8.5 Hz, quinolyl-H), 8.26–8.21 (m, 3H, phenyl-H, quinolyl-H), 8.17 (s, 1H, pyrimidine-H), 8.07 (d, 2H, ^3J = 8.9 Hz, phenyl-H), 7.93 (d, 1H, ^3J = 8.1 Hz,

quinolyl-H), 7.86 (m, 1H, quinolyl-H), 7.72 (m, 1H, quinolyl-H), 3.96 (s, 3H, CH_3), 3.83 (s, 3H, CH_3), 1.28 (s, 15H, Cp*–CH_3). ^{13}C NMR (101 MHz, $CDCl_3$) δ 168.91, 160.73, 156.61, 153.36, 149.78, 145.14, 139.69, 133.13, 131.10, 130.70, 129.80, 128.93, 128.67, 128.62, 126.83, 126.37, 122.41, 87.16, 60.53, 54.09, 8.62. FT-IR (KBr, cm^{-1}): ν = 1615 (C═O), 1580 (C═N), 1663 (C═N). (+)-HR-ESI-MS: *m/z* (%) 792.1824 ($[M - Cl]^+$, 100%), 828.1567 ($[M+H]^+$, 7%). HPLC purity: > 99%; $t_{r'}$ = 13.61 min.

4.5.5. C5

Dichloro(tetramethylphenylcyclopentadienyl)iridium(III) dimer (50.0 mg, 0.0540 mmol), **L2** (50.5 mg, 0.109 mmol) and $NaHCO_3$ (9.10 mg, 0.109 mmol) were reacted in methanol (1.50 mL) to afford complex **C5** as an orange powder in 75% yield (73.0 mg). ^{1}H NMR (300 MHz, $CDCl_3$): δ_H 8.46 (d, 1H, ^{3}J = 8.8 Hz, quinolyl-H), 8.34 (d, 1H, ^{3}J = 8.4 Hz, quinolyl-H), 8.27 (d, 1H, ^{3}J = 8.4 Hz, quinolyl-H), 8.17 (s, 1H, pyrimidine-H), 8.12 (d, 2H, ^{3}J = 9.0 Hz, phenyl-H), 8.06 (d, 2H, ^{3}J = 9.0 Hz, phenyl-H), 7.87 (d, 1H, ^{3}J = 8.3 Hz, quinolyl-H), 7.63–7.56 (m, 1H, quinolyl-H), 7.45–7.30 (m, 6H, Cp^x-phenyl-H, quinolyl-H), 3.97 (s, 3H, CH_3), 3.84 (s, 3H, CH_3), 1.50 (s, 3H, Cp^x-CH_3), 1.45 (s, 3H, Cp^x-CH_3), 1.41 (s, 3H, Cp^x-CH_3), 0.90 (s, 3H, Cp^x-CH_3). ^{13}C NMR (75 MHz, $CDCl_3$): δ_C 169.39, 160.89, 156.48, 153.44, 149.92, 145.11, 140.04, 133.64, 131.16, 131.02, 130.81, 130.07, 129.79, 129.07, 128.87, 128.66, 128.47, 127.12, 126.53, 122.66, 95.98, 95.86, 87.49, 83.49, 81.57, 60.69, 54.25, 10.27, 9.71, 8.66, 8.37. FT-IR (KBr, cm^{-1}): ν = 1622 (C═O), 1582 (C═N), 1663 (C═N). (+)-HR-ESI-MS: *m/z* (%) 854.2007 ($[M - Cl]^+$, 100%), 890.1763 ($[M+H]^+$, 22%). HPLC purity: 97.2%; $t_{r'}$ = 16.24 min.

4.5.6. C6

Dichloro(tetramethylbiphenylcyclopentadienyl)iridium(III) dimer (50.0 mg, 0.0470 mmol), **L2** (43.4 mg, 0.0930 mmol) and $NaHCO_3$ (7.80 mg, 0.0930 mmol) were reacted in methanol (1.50 mL) to afford complex **C6** as an orange powder in 56% yield (50.0 mg). ^{1}H NMR (400 MHz, $CDCl_3$): δ_H 8.47 (d, 1H, ^{3}J = 8.8 Hz, quinolyl-H), 8.34 (d, 1H, ^{3}J = 8.4 Hz, quinolyl-H), 8.28 (d, 1H, ^{3}J = 8.4 Hz, quinolyl-H), 8.17 (s, 1H, pyrimidine-H), 8.15 (d, 2H, ^{3}J = 8.9 Hz, phenyl-H), 8.07 (d, 2H, ^{3}J = 8.9 Hz, phenyl-H), 7.86 (d, 1H, ^{3}J = 8.2 Hz, quinolyl-H), 7.78 (s, 1H, sulfonamide-NH), 7.65–7.54 (m, 5H, quinolyl-H, Cp^x-phenyl-H), 7.51–7.44 (m, 2H, Cp^x-phenyl-H), 7.44 – 7.35 (m, 4H, quinolyl-H, Cp^x-phenyl-H), 3.97 (s, 3H, CH_3), 3.84 (s, 3H, CH_3), 1.52 (s, 3H, Cp^x-CH_3), 1.50 (s, 3H, Cp^x-CH_3), 1.40 (s, 3H, Cp^x-CH_3), 0.95 (s, 3H, Cp^x-CH_3).^{13}C NMR (101 MHz, $CDCl_3$): δ_C 169.40, 160.89, 156.49, 153.44, 149.92, 145.13, 141.16, 140.13, 140.06, 133.67, 131.02, 130.83, 130.22, 130.12, 130.06, 129.13, 129.08, 128.90, 128.66, 127.96, 127.62, 127.13, 127.06, 126.54, 122.68, 95.93, 95.73, 87.82, 83.37, 81.39, 60.69, 54.25, 10.34, 9.83, 8.64, 8.36. FT-IR (KBr, cm^{-1}): ν = 1623 (C═O), 1579 (C═N), 1661 (C═N). (+)-HR-ESI-MS: *m/z* (%) 930.2319 ($[M - Cl]^+$, 100%), 966.2080 ($[M+H]^+$, 18%). HPLC purity: 94%; $t_{r'}$ = 20.23 min.

4.6. X-ray crystallographic data collection

Crystals of **L1** were grown by layering a dichloromethane solution of **L1** with hexane and left to stand in a sealed vial for several days at room temperature. A crystal of diffraction quality was selected for analysis and mounted in oil. Low temperature X-ray diffraction data collection for **L1** was performed at 100(2) K on a Bruker APEX II DUO CCD diffractometer using graphite-monochromated MoKα radiation (0.71073 Å). An Oxford Cryostream plus, 700 series cryostat that was attached to the diffractometer cooled the sample. Data were collected up to 55.1° 2θ. Lp and absorption corrections applied, μ = 0.221 mm^{-1}. Bruker diffraction, SAINT [64] software was used for data reduction and unit cell determinations, while SADABS [51,65] was used for absorption corrections. SHELXL-16 [66] and SHELXT-14 [66] was used to refine and solve crystal structures with the X-seed [67,68] graphical user interface. Calculated positions were used to place hydrogen atoms and non-hydrogen atoms were refined anisotropically. Hydrogens on oxygen and nitrogen atoms were located with electron density maps. Crystal data, structure refinement parameters and selected bonds and angles are summarised in Table 1 and Table 2.

4.7. HPLC purity determination

Purity measurements by HPLC were carried out using the Agilent 1220 system with a DAD and 100 μL loop. The column used was a Kinetex® 5 μm C18 100 Å, 150 × 4.6 mm with a 5 μm pore size. The mobile phase was H_2O 0.1% TFA (A) / MeCN 0.1% TFA (B). Elution was carried out using gradient: t = 0 min 10% B, t = 30 min 80% B, t = 40 min 80% B, t = 41 min 10% B, and t = 55 min 10% B over a 55 min period. The flow rate was 1 mL·min^{-1}, and the detection wavelength was set at 254 nm and 400 nm with the reference wavelength at 360 nm. Samples were dissolved in 10% MeCN/90% H_2O at *ca.* 100 μM. Sample injections were half the loop volume (50 μL) with needle washes of MeCN and H_2O between injections. It was assumed that all species in a sample have the same extinction coefficient at 254 nm and 400 nm. All peaks were manually integrated.

4.8. General procedure for generation of aqua species with $AgNO_3$

The complex was stirred for 18 h with an equimolar quantity of $AgNO_3$ in deuterium oxide (1.20 mL) at 37 °C in an oil bath. The solution was subsequently filtered through a plug of Celite™ and collected in an NMR tube and 1–2 drops of TMS added as internal standard. Solutions were then analysed with ^{1}H NMR.

4.8.1. C1-D_2O

(9.30 mg, 1.20 × 10^{-2} mmol) and $AgNO_3$ (2.10 mg, 1.20 × 10^{-2} mmol) were reacted in D_2O (1.20 mL). ^{1}H NMR (400 MHz, D_2O) δ 9.01 (d, 1H, ^{3}J = 5.4 Hz, pyridyl-H), 8.30–8.24 (m, 1H, pyridyl-H), 8.16–8.06 (m, 4H, pyridyl-H, pyrimidine-H, phenyl-H), 7.91–7.85 (m, 1H, pyridyl-H), 7.46 (d, 2H, ^{3}J = 8.9 Hz, phenyl-H), 3.99 (s, 3H, CH_3), 3.83 (s, 3H, CH_3), 1.27 (s,15H, Cp*–CH_3).

4.8.2. C2-D_2O

(10.0 mg, 1.20 × 10^{-2} mmol) and $AgNO_3$ (2.10 mg, 1.20 × 10^{-2} mmol) were reacted in D_2O (1.20 mL). ^{1}H NMR (400 MHz, D_2O): δ_H 8.94 (d, 1H, ^{3}J = 5.4 Hz, pyridyl-H), 8.31 (m, 1H, pyridyl-H), 8.17 (d, 1H, ^{3}J = 7.6 Hz, pyridyl-H), 8.04 (s, 1H, pyrimidine-H), 7.92 (d, 2H, ^{3}J = 8.6 Hz, phenyl-H), 7.85 (m, 1H, pyridyl-H), 7.47 (t, 1H, ^{3}J = 7.7 Hz, Cp^x-phenyl-H), 7.36 (t, 2H, ^{3}J = 7.7 Hz, phenyl-H), 7.18(d, 2H, ^{3}J = 8.6 Hz, phenyl-H), 7.12 (d, 2H, ^{3}J = 7.7 Hz, Cp^x-phenyl-H), 4.03 (s, 3H, CH_3), 3.80 (s, 3H, CH_3), 1.58 (s, 6H, Cp^x-CH_3), 1.09 (s, 6H, Cp^x-CH_3).

4.8.3. C4-D_2O

(9.90 mg, 1.20 × 10^{-2} mmol) and $AgNO_3$ (2.00 mg, 1.20 × 10^{-2} mmol) were reacted in D_2O (1.20 mL). ^{1}H NMR (400 MHz, D_2O): δ_H 8.79 (d, 1H, ^{3}J = 8.6 Hz, quinolyl-H), 8.50 (d, 1H, ^{3}J = 9.0 Hz, quinolyl-H), 8.23 (d, 1H, ^{3}J = 8.2 Hz, quinolyl-H) 8.14–8.20 (m, 2H, quinolyl-H), 8.03 (d, 2H, ^{3}J = 8.5 Hz, phenyl-H), 7.90–7.97 (m, 2H, quinolyl-H, pyrimidine-H), 7.67 (d, 2H, ^{3}J = 8.5 Hz, phenyl-H), 3.94 (s, 3H, CH_3), 3.82 (s, 3H, CH_3), 1.19 (s, 15H, Cp*–CH_3).

4.9. General procedure for generation of aqua complexes without $AgNO_3$

The complex was dissolved in deuterated acetone (300 μL) and then mixed with deuterium oxide (900 μL) in a vial for a final solution of 25% (v/v) deuterated acetone/deuterium oxide (1.20 mL). The resultant mixture was then stirred for 18 h at 37 °C in an oil bath. The solution was subsequently filtered through a plug of Celite™ and collected in an NMR tube and 1–2 drops of TMS was added as internal standard. Samples were analysed with ^{1}H NMR and then submitted for ESI-mass

spectrometry analysis.

4.10. M. tuberculosis MIC determination assay.

The minimum inhibitory concentration (MIC) was determined using the standard broth micro dilution method, as described previously. Briefly, a 10 mL culture of *Mycobacterium tuberculosis* pMSp12::GFP [69-71] was grown to an optical density (OD600) of 0.6 – 0.7. Cultures were diluted prior to inoculation of assays, as follows: (i) 1:100 in Gaste-Fe (glycerol–alanine–salts) medium pH 6.6, supplemented with 0.05% Tween-80 and 1% Glycerol [72,73]; (ii) 1:500 in 7H9 supplemented with 10% Albumin Dextrose Catalase supplement (ADC), 0.4% Glucose and 0.05% Tween-80.[72,73] The compounds to be tested were reconstituted in DMSO.

Two-fold serial dilutions of the test compound were prepared across a 96-well microtitre plate, after which 50 μL of the diluted *M. tuberculosis* cultures were added to each well in the serial dilution. The plate layout was a modification of the method previously described [74]. Assay controls used were a minimum growth control (Rifampicin at 2xMIC), and a maximum growth control (5% DMSO).

The microtitre plates were sealed in a secondary container and incubated at 37 °C with 5% CO_2 and humidification. Relative fluorescence (excitation 485 nm; emission 520 nm) was measured using a plate reader (FLUOstar OPTIMA, BMG LABTECH), at day 7 and day 14. The raw fluorescence data were archived and analysed using the CDD Vault from Collaborative Drug Discovery, in which, data are normalised to the minimum and maximum inhibition controls to generate a dose response curve (% inhibition), using the Levenberg-Marquardt damped least-squares method, from which the MIC_{90} is calculated (The Collaborative Drug Discovery database, Burlingame, CA www.collaborativedrug.com). The lowest concentration of drug that inhibits growth of >90% of the bacterial population is considered to be the MIC_{90}.

4.11. Evaluation of in vitro activity against P. falciparum asexual blood stages [75]

Stock solutions of the compounds to be tested were prepared in DMSO (20 mM). The stock solutions were further diluted in 384-well polypropylene microtitre plates to produce 3 doses per log dose response with final assay concentrations of the compounds ranging between 80 μM and 0.8 nM. A 1:25 dilution was then made of the compound plates with sterile water in a 384-well polystyrene plate and 5 μL of these wells were then transferred into a 384-well imaging plate. 4% DMSO and 50 μM Puromycin were used as controls under the same conditions and dilutions as that of the compounds.

A Plasmodium falciparum standard genomic reference strain (3D7), multidrug resistant strain (Dd2) and gametocyte forming pyrimethamine resistant and chloroquine sensitive strain (HB3) were cultured within the medium RPMI-1640 which was supplemented with 10 mM HEPES, 25 μg/mL hypoxanthine, 5% human serum and 2.5 mg/mL Albumax while being incubated at 37 °C under 5% CO_2, 5% O_2 and 90% N_2. Sorbitol synchronization was performed twice, consecutively, during the intra-erythrocytic lifecycles to provide ring-stage parasites for the assays [76]. The ring stage parasite culture had its percentage parasitaemia and percentage haematocrit adjusted to 2% and 0.3%, respectively, and thereafter 45 μL of the adjusted parasite culture was added to compound containing imaging plates prepared as described earlier. The imaging plates were then incubated for 72 h under the same conditions as described for the original cultures. The plates were then stained with 4′,6-diamidino-2-phenylindole (DAPI) and incubated overnight at room temperature before being imaged on an Opera confocal high content imaging system. Accapella scripting software was used to determine the number of classified parasites which was subsequently normalized to obtain the percentage inhibition with regards to the two plate controls, 0.4% DMSO and 5 μM Puromycin. The normalized inhibition data was then plotted against the log concentration of the compounds using GraphPad Prism 4.0, and the non-linear regression, sigmoidal dose response variable slope and the IC_{50} determined (where two or more points formed a plateau in the software). The data was generated from two biological replicates in duplicate of the three strains used.

4.12. Human embryonic kidney (HEK293) mammalian cell cytotoxicity

HEK293 cells were cultured in DMEM culture media supplemented with 10% Foetal Bovine Serum (FBS). The cells were harvested and dispensed into 384 well sterile black, clear base microtitre plates at 2000 cells/well (45 μL). The plates were left to settle, and the cells attach overnight in a standard tissue culture incubator at 5% CO_2, 37 °C and 60% humidity. After overnight incubation, 5 μL of diluted compound (as described in the section, Evaluation of *in vitro* activity against *P. falciparum* asexual blood stages) was added to the cell containing plates and incubated for a further 72 h. After incubation the supernatant from the wells was removed and 40ul of 40 μM resazurin in DMEM media (FBS free) added to all wells. The plates were incubated for 6 h then measured for fluorescent intensity using the PerkinElmer Envision. The data were analysed as in the *Plasmodium falciparum* methods section.

Declaration of Competing Interest

The authors declare that they have no known competing financial interests or personal relationships that could have appeared to influence the work reported in this paper.

Acknowledgements

We thank the National Research Foundation (NRF) of South Africa (Thuthuka grant: 106952). Research reported in this publication was supported by the Strategic Health Innovation Partnerships (SHIP) Unit of the South African Medical Research Council with funds received from the South African Department of Science Innovation (to D.F.W.). This study was also supported by the Australian Research Council (LP120200557 award to V.M.A.). We thank the Australian Red Cross Blood Bank for the provision of fresh red blood cells, without which the *Plasmodium falciparum* research could not have been performed. This work was also supported by the National Health and Medical Research Council Postgraduate Scholarship (NHMRC APP1150359), a Griffith University Postgraduate Scholarship and Discovery Biology Postgraduate Scholarship all awarded to Sandra Duffy.

Appendix A. Supplementary data

Appendix A contains the supplementary data for this paper. CCDC 1949937 contains the crystallographic data for this article, in CIF format. These data can be obtained free of charge at www.ccdc.cam.ac.uk/conts/retrieving.html [or from the Cambridge Crystallographic Data Centre, 12, Union Road, Cambridge CB2 1EZ, UK; fax: (internat.) +44-1223/336-033; E-mail: deposit@ccdc.cam.ac.uk]. Supplementary data to this article can be found online at https://doi.org/10.1016/j.ica.2020.120175.

References

[1] World Health Organization, Global Tuberculosis Report, 2019.
[2] E.A. Hillard, G. Jaouen, Organometallics 30 (1) (2011) 20–27.
[3] W. Castro, M. Navarro, C. Biot, Future Med. Chem. 5 (1) (2013) 81–96.
[4] A.H. Ngo, S. Bose, L.H. Do, Chem. Eur. J. 24 (42) (2018) 10584–10594.
[5] K. Na-Bangchang, J. Karbwang, Fund. Clin. Pharmacol. 23 (4) (2009) 387–409.
[6] F.P. L'Abbate, R. Müller, R. Openshaw, J.M. Combrinck, K.A. de Villiers, R. Hunter, T.J. Egan, Eur. J. Med. Chem. 159 (2018) 243–254.
[7] M. Rizzotto, Metal Complexes as Antimicrobial Agents, in: V. Bobbarala (Ed.), A Search for Antibacterial Agents, IntechOpen2012.
[8] P.C.A. Bruijnincx, P.J. Sadler, Curr. Opin. Chem. Biol. 12 (2) (2008) 197–206.

[9] J.A. Obaleye, A.C. Tella, M.O. Bamigboye, Metal Complexes as Prospective Antibacterial Agents, in: V. Bobbarala (Ed.), A Search for Antibacterial Agents, IntechOpen2012.
[10] M. Navarro, W. Castro, C. Biot, Organometallics 31 (16) (2012) 5715–5727.
[11] N. Chavain, C. Biot, Curr. Med. Chem. 17 (25) (2010) 2729–2745.
[12] T.I. Kostelnik, C. Orvig, Chem. Rev. 119 (2) (2019) 902–956.
[13] C. Zhen-Feng, C. Orvig, L. Hong, Curr. Top. Med. Chem. 17 (28) (2017) 3131–3145.
[14] K.D. Mjos, C. Orvig, Chem. Rev. 114 (8) (2014) 4540–4563.
[15] P. Chellan, V.M. Avery, S. Duffy, J.A. Triccas, G. Nagalingam, C. Tam, L.W. Cheng, J. Liu, K.M. Land, G.J. Clarkson, I. Romero-Canelón, P.J. Sadler, Chem. Eur. J. 24 (40) (2018) 10078–10090.
[16] M. Navarro, C. Gabbiani, L. Messori, D. Gambino, Drug Discov. Today 15 (23) (2010) 1070–1078.
[17] A. van Niekerk, P. Chellan, S.F. Mapolie, Eur. J. Inorg. Chem. 2019 (30) (2019) 3432–3455.
[18] P. Chellan, T. Stringer, A. Shokar, A. Au, C. Tam, L.W. Cheng, G.S. Smith, K. M. Land, Inorg. Chem. Commun. 102 (2019) 1–4.
[19] E. Ekengard, L. Glans, I. Cassells, T. Fogeron, P. Govender, T. Stringer, P. Chellan, G.C. Lisensky, W.H. Hersh, I. Doverbratt, S. Lidin, C. de Kock, P.J. Smith, G. S. Smith, E. Nordlander, Dalton Trans. 44 (44) (2015) 19314–19329.
[20] P. Chellan, K.M. Land, A. Shokar, A. Au, S.H. An, D. Taylor, P.J. Smith, T. Riedel, P. J. Dyson, K. Chibale, G.S. Smith, Dalton Trans. 43 (2) (2014) 513–526.
[21] P. Chellan, K.M. Land, A. Shokar, A. Au, S.H. An, D. Taylor, P.J. Smith, K. Chibale, G.S. Smith, Organometallics 32 (17) (2013) 4793–4804.
[22] F. Dubar, C. Slomianny, J. Khalife, D. Dive, H. Kalamou, Y. Guérardel, P. Grellier, C. Biot, Angew. Chem. Int. Ed. 52 (30) (2013) 7690–7693.
[23] J. Hess, G. Panic, M. Patra, L. Mastrobuoni, B. Spingler, S. Roy, J. Keiser, G. Gasser, A.C.S. Infect, Dis. 3 (9) (2017) 645–652.
[24] E.V. Capparelli, R. Bricker-Ford, M.J. Rogers, J.H. McKerrow, S.L. Reed, Antimicrob Agents Chemother 61 (1) (2016) e01947–16.
[25] S. Vale-Costa, N. Vale, J. Matos, A. Tomás, R. Moreira, P. Gomes, M.S. Gomes, Antimicrob. Agents Chemother. 56 (11) (2012) 5774–5781.
[26] J. Lecina, P. Cortés, M. Llagostera, C. Piera, J. Suades, Bioorg. Med. Chem. 22 (13) (2014) 3262–3269.
[27] G. Jaouen, A. Vessières, S. Top, Chem. Soc. Rev. 44 (24) (2015) 8802–8817.
[28] B. Reta, B. Erko, Trop. Med. Int. Health 18 (11) (2013) 1338–1343.
[29] M. Patra, K. Ingram, A. Leonidova, V. Pierroz, S. Ferrari, M.N. Robertson, M. H. Todd, J. Keiser, G. Gasser, J. Med. Chem. 56 (22) (2013) 9192–9198.
[30] J. Hess, M. Patra, V. Pierroz, B. Spingler, A. Jabbar, S. Ferrari, R.B. Gasser, G. Gasser, Organometallics 35 (19) (2016) 3369–3377.
[31] B. Xing, C.-W. Yu, P.-L. Ho, K.-H. Chow, T. Cheung, H. Gu, Z. Cai, B. Xu, J. Med. Chem. 46 (23) (2003) 4904–4909.
[32] L.C. Eiter, N.W. Hall, C.S. Day, G. Saluta, G.L. Kucera, U. Bierbach, J. Med. Chem. 52 (21) (2009) 6519–6522.
[33] E.H.S. Sousa, L.A. Basso, D.S. Santos, I.C.N. Diógenes, E. Longhinotti, L.G. de França Lopes, Í. de Sousa Moreira, J. Biol. Inorg. Chem. 17 (2) (2012) 275–283.
[34] R.J. Henry, Bacteriol. Rev 7 (4) (1943) 175–262.
[35] A. Kołaczek, I. Fusiarz, J. Lawecka, D. Branowska, Chemik 68 (7) (2014) 620–628.
[36] E.E. Connor, Prim. Care Update Ob. Gyns. 5 (1) (1998) 32–35.
[37] T.H. Maren, Annu. Rev. Pharmacol. Toxicol. 16 (1) (1976) 309–327.
[38] T. Owa, T. Nagasu, Expert Opin. Ther. Pat. 10 (11) (2000) 1725–1740.
[39] A. Kleemann, J. Engel, B. Kutscher, D. Reichert, Pharmaceutical Substances: Syntheses, Patents, Applications, 1st ed., Thieme, Stuttgart, 1999.
[40] W.R. Roush, S.L. Gwaltney, J. Cheng, K.A. Scheidt, J.H. McKerrow, E. Hansell, J. Am. Chem. Soc. 120 (42) (1998) 10994–10995.
[41] A. Burger, M. Wolff, Burger's Medicinal Chemistry and Drug Discovery, 1st ed., Wiley, New York, 1995.
[42] P. Forgacs, N.L. Wengenack, L. Hall, S.K. Zimmerman, M.L. Silverman, G. D. Roberts, Antimicrob. Agents Chemother. 53 (11) (2009) 4789.
[43] E. Kremer, G. Facchin, E. Estévez, P. Alborés, E.J. Baran, J. Ellena, M.H. Torre, J. Inorg. Biochem. 100 (7) (2006) 1167–1175.
[44] C.M. Sharaby, M.F. Amine, A.A. Hamed, J. Mol. Struct. 1134 (2017) 208–216.
[45] L.-J. Ming, Med. Res. Rev. 23 (6) (2003) 697–762.
[46] H. Keypour, M. Shayesteh, M. Rezaeivala, F. Chalabian, Y. Elerman, O. Buyukgungor, J. Mol. Struct. 1032 (2013) 62–68.
[47] M. Mondelli, V. Bruné, G. Borthagaray, J. Ellena, O.R. Nascimento, C.Q. Leite, A. A. Batista, M.H. Torre, J. Inorg. Biochem. 102 (2) (2008) 285–292.
[48] R.R. Coombs, M.K. Ringer, J.M. Blacquiere, J.C. Smith, J.S. Neilsen, Y.-S. Uh, J. B. Gilbert, L.J. Leger, H. Zhang, A.M. Irving, S.L. Wheaton, C.M. Vogels, S. A. Westcott, A. Decken, F.J. Baerlocher, Transit. Met. Chem. 30 (4) (2005) 411–418.
[49] M. Zaki, F. Arjmand, S. Tabassum, Inorg. Chim. Acta 444 (2016) 1–22.
[50] Z.H. Chohan, H.A. Shad, J. Enzyme Inhib. Med. Chem. 27 (3) (2012) 403–412.
[51] Z.H. Chohan, H.A. Shad, M.H. Youssoufi, T. Ben Hadda, Eur. J. Med. Chem. 45 (7) (2010) 2893–2901.
[52] Z.H. Chohan, H. Mahmood ul, K.M. Khan, C.T. Supuran, J. Enzyme Inhib. Med. Chem. 20 (2) (2005) 183–188.
[53] N.U. Hassan Khan, S. Zaib, K. Sultana, I. Khan, B. Mougang-Soume, H. Nadeem, M. Hassan, J. Iqbal, RSC Adv. 5 (38) (2015) 30125–30132.
[54] A. Nocentini, M. Ferraroni, F. Carta, M. Ceruso, P. Gratteri, C. Lanzi, E. Masini, C. T. Supuran, J. Med. Chem. 59 (23) (2016) 10692–10704.
[55] C. Yenikaya, H. İlkimen, M.M. Demirel, B. Ceyhan, M. Bülbül, E. Tunca, J. Braz. Chem. Soc. 27 (2016) 1706–1714.
[56] E. Bruno, M.R. Buemi, A. Di Fiore, L. De Luca, S. Ferro, A. Angeli, R. Cirilli, D. Sadutto, V. Alterio, S.M. Monti, C.T. Supuran, G. De Simone, R. Gitto, J. Med. Chem. 60 (10) (2017) 4316–4326.
[57] M. Mondelli, F. Pavan, P.C. de Souza, C.Q. Leite, J. Ellena, O.R. Nascimento, G. Facchin, M.H. Torre, J. Mol. Struct. 1036 (2013) 180–187.
[58] C. Quintana, G. Silva, A.H. Klahn, V. Artigas, M. Fuentealba, C. Biot, I. Halloum, L. Kremer, N. Novoa, R. Arancibia, Polyhedron 134 (2017) 166–172.
[59] P. Doig, P.A. Boriack-Sjodin, J. Dumas, J. Hu, K. Itoh, K. Johnson, S. Kazmirski, T. Kinoshita, S. Kuroda, T.-O. Sato, K. Sugimoto, K. Tohyama, H. Aoi, K. Wakamatsu, H. Wang, Bioorg. Med. Chem. 22 (21) (2014) 6256–6269.
[60] Q. Li, S.-Y. Zhang, G. He, Z. Ai, W.A. Nack, G. Chen, Org. Lett. 16 (6) (2014) 1764–1767.
[61] Ü.Ö. Özdemir, P. Güvenç, E. Şahin, F. Hamurcu, Inorg. Chim. Acta 362 (8) (2009) 2613–2618.
[62] S.-N. Li, Q.-G. Zhai, M.-C. Hu, Y.-C. Jiang, Inorg. Chim. Acta 362 (7) (2009) 2217–2221.
[63] J. Tönnemann, J. Risse, Z. Grote, R. Scopelliti, K. Severin, Eur. J. Inorg. Chem. 2013 (26) (2013) 4558–4562.
[64] A. Çapcı, M.M. Lorion, H. Wang, N. Simon, M. Leidenberger, M.C. Borges Silva, D. R.M. Moreira, Y. Zhu, Y. Meng, J.Y. Chen, Y.M. Lee, O. Friedrich, B. Kappes, J. Wang, L. Ackermann, S.B. Tsogoeva, Angew. Chem. Int. Ed. 58 (37) (2019) 13066–13079.
[65] R. Blessing, Acta Cryst. A 51 (1) (1995) 33–38.
[66] G.M. Sheldrick, Acta Cryst. C 71 (1) (2015) 3–8.
[67] L.J. Barbour, J. Supramol. Chem. 1 (4) (2001) 189–191.
[68] J.L. Atwood, L.J. Barbour, Crys. Growth Des. 3 (1) (2003) 3–8.
[69] G.L. Abrahams, A. Kumar, S. Savvi, A.W. Hung, S. Wen, C. Abell, C.E. Barry, D. R. Sherman, H.I.M. Boshoff, V. Mizrahi, Chem. Biol. 19 (7) (2012) 844–854.
[70] L. Collins, S.G. Franzblau, Antimicrob Agents Chemother 41 (5) (1997) 1004–1009.
[71] L.A. Collins, M.N. Torrero, S.G. Franzblau, Antimicrob. Agents Chemother. 42 (2) (1998) 344–347.
[72] J.J. De Voss, K. Rutter, B.G. Schroeder, H. Su, Y. Zhu, C.E. Barry, 3rd, Proc. Natl. Acad. Sci. U S A 97(3) (2000) 1252-1257.
[73] S.G. Franzblau, M.A. DeGroote, S.H. Cho, K. Andries, E. Nuermberger, I.M. Orme, K. Mdluli, I. Angulo-Barturen, T. Dick, V. Dartois, A.J. Lenaerts, Tuberculosis 92 (6) (2012) 453–488.
[74] J. Ollinger, M.A. Bailey, G.C. Moraski, A. Casey, S. Florio, T. Alling, M.J. Miller, T. Parish, PLOS ONE 8 (4) (2013), e60531.
[75] S. Duffy, V.M. Avery, Am J Trop Med Hyg 86 (1) (2012) 84–92.
[76] C. Lambros, J.P. Vanderberg, J. Parasitol. 65 (3) (1979) 418–420.